Nonlinear Dyn (2022) 110:257–279
https://doi.org/10.1007/s11071-022-07659-1

ORIGINAL PAPER

Nonlinear dynamics analysis of multifactor low-speed heavy-load gear system with temperature effect considered

Jungang Wang · Zheng'ang Shan · Sheng Chen

Received: 5 December 2021 / Accepted: 17 June 2022 / Published online: 29 June 2022

Abstract Low-speed and heavy-load gears generate a lot of heat during meshing transmission, which leads to thermal deformation of the gears and affects the transmission performance of the gear system. It is of great significance to explore the influence law of temperature effects on the nonlinear dynamics of the gear system. Based on the principle of thermal deformation, taking into account the temperature effect and nonlinear parameters, including time-varying meshing stiffness, tooth side clearance as well as comprehensive errors, a nonlinear dynamic model of the gear system of spur cylindrical gear system is established. The Runge–Kutta method is used for numerical solution, the effect of temperature variation and time-varying stiffness coefficient on the bifurcation characteristics of the gear system is analyzed by combining bifurcation diagram, maximum Lyapunov index diagram, phase diagram and Poincare section diagram. The results show that the gear system exhibits complex nonlinear dynamics with the consideration of temperature effects, including four states of single-fold periodic motion, multi-fold periodic motion, and bifurcation and chaotic motion. The influence of temperature variation on the nonlinear characteristics of the gear system is closely related to the value of the time-varying stiffness coefficient. The effect of temperature variation on the bifurcation characteristics of the system is obvious when the value of the time-varying stiffness coefficient s is in the range of $0.4 < s < 0.8$. The relevant conclusions can provide references for the design of gear systems under special working conditions.

Keywords Temperature effect · Nonlinear dynamics · Bifurcation diagram · Largest Lyapunov exponent graph · Time-varying meshing stiffness

J. Wang (✉) · Z. Shan · S. Chen
Key Laboratory of Conveyance and Equipment, Ministry of Education, East China Jiaotong University, Nanchang, China
e-mail: mewjg@ecjtu.edu.cn

Z. Shan
e-mail: shanzhengang111@163.com

S. Chen
e-mail: 1748486758@qq.com

1 Introduction

Gear system is a kind of transmission mechanism with high efficiency, stable operation and high transmission accuracy, which is widely used in aerospace, high-speed trains, power generation and other industries. During the operation of a gear system, nonlinear excitation can cause the system to enter an unstable state of motion and can even lead to an increase in error and noise as well as premature failure of the gear. Therefore, the study of the dynamic characteristics of the gear system and the analysis of the influence law of each parameter on the stability of the system can not

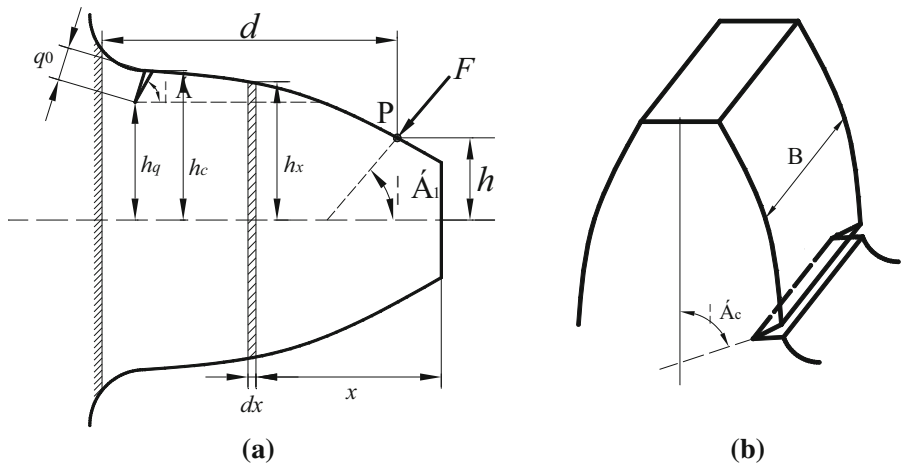

Fig. 1 Cantilever beam model

only improve the accuracy of the gear system, but also improve the working condition of the gear, thus extending the gear life.

Gearing systems are widely applied in a variety of fields, and a number of scholars have conducted nonlinear dynamics studies on gearing systems for different application scenarios. Wang et al. [1] developed a torsional nonlinear dynamics model of an aero-engine drive train, solved and analyzed the dynamic response using Runge–Kutta method, and proved the existence of different nonlinear dynamic characteristics of the gear system by bifurcation diagram and FFT spectrum. Zhao et al. [2] studied gear systems in wind turbines and showed that meshing shock stresses and time-varying meshing stiffness have an effect on dynamic transmission errors. Hou et al. [3] developed a nonlinear model of the gear-rotor of a geared turbofan engine and they used bifurcation chart, maximum Lyapunov index chart, and Poincare cross-section chart to illustrate the nonlinear response and analyze the effect of damping on the kinematic state of the system. Low-speed and heavy-load gears are mainly used in the coal mining industry. As a result of the harsh working environment, the gear system generates violent vibration during operation, which affects the life of the gears, Jiang et al. [4] developed a nonlinear dynamics model of the coal mining machine gear system and studied the dynamic response of the gear system by numerical analysis methods. Chen et al. [5] established a nonlinear dynamics model of the coal mining machine gear system with consideration of thermal deformation. They obtained the influence of temperature on the nonlinear characteristics of the system. Low-speed heavy-duty gears are prone to abnormal gear system operation due to their harsh operating environment, so it is essential to investigate their nonlinear dynamics. Aiming to investigate the nonlinear dynamics of gear systems more deeply and improve the stability of gear systems, a number of scholars have used different approaches to establish dynamics models to study gear systems. Huang et al. [6] used the concentrated mass approach to model the dynamics of a gear system with multiple clearances. They investigated the effects of excitation frequency, gear clearance and other parameters on the nonlinear dynamic characteristics of the system. Zhang et al. [7] developed a dynamics model based on Hertz contact theory and fractal theory. They obtained the effect law of parameters like tooth side clearance and time-varying meshing stiffness on the change of system motion state by considering various factors. Wang et al. [8] developed the vibration equation of the gear train according to Newton's law. They obtained the effect of random parameters on the dynamic response of the gear system under different operating conditions by solving it. Geng et al. [9] developed a nonlinear dynamics model with consideration of surface friction, time-varying tooth gap and meshing stiffness to study the bifurcation properties of the gear system in depth by bifurcation diagrams and spectrograms. Liu et al. [10] studied the nonlinear characteristics of a gear system under constant and variable excitation. They showed the influence of gear speed on the dynamic characteristics

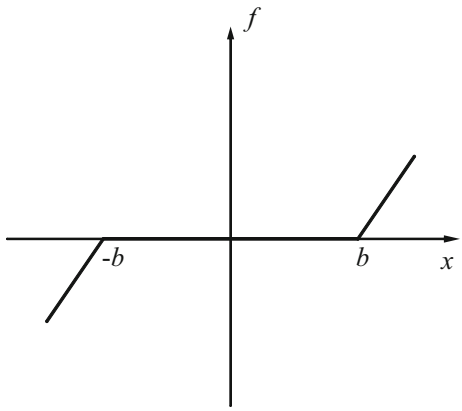

Fig. 2 Nonlinear function of tooth side clearance

of the gear system using bifurcation diagrams. Liu et al. [11] developed a nonlinear dynamics model considering thermal deformation and analyzed the effect of temperature variation on the nonlinear dynamic properties of the system using spectrograms, and the results indicated that the vibration displacement and load of the system are enhanced at higher temperatures. Wang et al. [12] developed a gear system model with consideration of tooth clearance, load distribution, time-varying meshing stiffness, etc. The analysis using numerical analysis showed that periodic, quasi-periodic and chaotic motion states exist in the gear system, and the rotational speed has obvious influences on the vibration characteristics. Wang et al. [13] developed dynamic equations with consideration of nonlinear factors such as torque fluctuation, mesh damping ratio, and excitation frequency, and analyzed the dynamic properties of the gear system with different tooth clearances for changes in the mesh damping ratio using the bifurcation chart, phase chart, and Poincare chart of the system. Xiang et al. [14, 15] proposed a transverse torsion model for a multistage transmission system and analyzed the nonlinear dynamic response using excitation frequency and support stiffness as bifurcation factors, and the findings showed that the system exhibits diverse motion states under the variation of support stiffness, and the motion at low and high excitation frequencies and the route into the chaotic state are different. Li et al. [16] considered the dynamic response of a single-degree-of-freedom system with nonlinear stiffness and damping. They described the effects of amplitude and relative phase for two types of excitation as well as bifurcation analysis. Neumeyer et al. [17, 18] derived approximate steady-state vibration amplitudes by using the method of varying amplitudes, which is in good agreement with the results of numerical integration, and obtained approximate analytical steady-state solutions and consequent stability by varying the amplitudes. Zhu et al. [19] developed dynamic equations with multiple tooth gaps and time-varying meshing stiffness. They analyzed the influence of tooth gaps on the dynamic properties of the gear set by combining the time-domain chart, phase chart and Poincare section chart. For gears in extreme operating conditions and precision transmission mechanisms, changes in temperature and power loss can cause changes in tooth side clearance, which can affect the dynamic performance of gears [20]. Most of the existing studies have ignored the effect of temperature, and rarely considered the effect law of temperature on the nonlinear properties of gear systems. And studies on the bifurcation properties of the system considering parameters including temperature variation, time-varying stiffness and engagement damping simultaneously are lacking.

In this paper, a nonlinear dynamics model of gear system considering temperature effect is established based on the principle of thermal deformation, and considering the time-varying meshing stiffness, tooth side clearance and meshing error etc. And the bifurcation characteristics of nonlinear systems are analyzed by bifurcation diagram, maximum Lyapunov index diagram, time-domain diagram, phase diagram, spectrum diagram and Poincare cross-section diagram to study the influence law of temperature variation, time-varying meshing stiffness and other factors on the bifurcation characteristics of the system, which provides a reference for the design and application of gear systems under special working conditions.

2 Nonlinear dynamics model of multi-factor gear system considering temperature effect

The gear system consists of several gear pairs and drive shafts, bearings and other parts of the mechanical system, under the action of dynamic excitation will produce dynamic response, generate vibration and noise, and the system is subject to dynamic excitation is not only related to the structure of the gear itself, geometric characteristics and error state, etc., but also

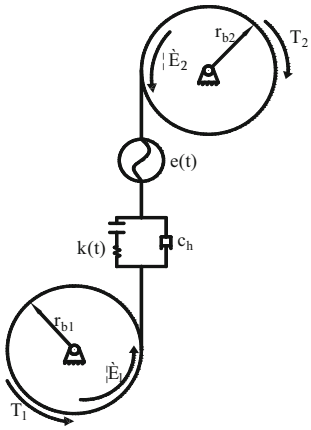

Fig. 3 Dynamics model of spur gear system

related to the excitation of other parts in the gear system. Therefore, to analyze the nonlinear dynamics of the gear system, it is necessary to start from the system as a whole and establish an overall vibration analysis model.

2.1 Time-varying meshing stiffness of gears

The potential energy approach is used to assume the gear model as a cantilever beam model, and the time-varying meshing stiffness of normal teeth is determined by considering the Hertzian contact effect, the bending effect and the axial compression effect. The cantilever beam model is shown in Fig. 1.

When the gear teeth are engaged, the tooth deformation at the line of engagement at point P under the action of the engagement force F is subject to three influencing factors: (1) local stiffness due to Hertzian contact K_h; (2) the basic deflection of the tooth, including the bending stiffness K_b, the shear stiffness K_s and the axial compression stiffness K_a; (3) deflection due to gear tooth flexibility K_f.

$$\begin{cases} \dfrac{1}{K_b} = \displaystyle\int_0^d \frac{(x\cos\alpha_1 - h\sin\alpha_1)^2}{EI_x}dx \\ \dfrac{1}{K_s} = \displaystyle\int_0^d \frac{1.2\cos^2\alpha_1}{GA_x}dx \\ \dfrac{1}{K_a} = \displaystyle\int_0^d \frac{\sin^2\alpha_1}{EA_x}dx \\ \dfrac{1}{K_h} = \dfrac{4(1-v^2)}{\pi EB} \\ \dfrac{1}{K_f} = \dfrac{\delta_f}{F} \end{cases} \tag{1}$$

where d is the distance from the point of load action along the tooth height direction; α_1 is the pressure angle; h is the distance from the point of load action along the tooth width; E is Young's modulus of elasticity; I_x,A_x are the cross-sectional moment of inertia and integral cross-sectional area, respectively, for gear teeth without cracks, I_x,A_x follows the whole tooth integral,$I_x = \frac{1}{12}(h_x + h_x)^3 B$,$A_x = (h_x + h_x)B$; G is the shear modulus,$G = \frac{E}{2(1+v)}$; v is the Poisson's ratio; B is the tooth width; δ_f is the deformation of the gear base body caused by the load.

The combined time-varying rigidity of a single pair of teeth meshing is expressed as:

$$K_e = \frac{1}{\frac{1}{K_h} + \frac{1}{K_{b_1}} + \frac{1}{K_{s_1}} + \frac{1}{K_{a_1}} + \frac{1}{K_{f_1}} + \frac{1}{K_{b_2}} + \frac{1}{K_{s_2}} + \frac{1}{K_{a_2}} + \frac{1}{K_{f_2}}} \tag{2}$$

In the formula: K_{b_1},K_{b_2} is the bending stiffness of the driving wheel and the driven wheel;K_{s_1},K_{s_2} is the shear stiffness of the driving wheel and the driven wheel; K_{a_1},K_{a_2} is the axial compression stiffness of the driving wheel and the driven wheel; K_{f_1},K_{f_2} is the deflection generated by the gear base bodies of the driving wheel and the driven wheel.

When a gear meshes, its meshing rigidity is not a fixed number, but is continuously varying with time, and this variation is called the time-varying rigidity, and the excitation phenomenon that it causes is called the rigidity excitation of the gear teeth. Since the transmission of gears is a periodic motion, the meshing rigidity is a periodic function with certain regularity. The stiffness of each discrete point is found in turn and combined to obtain the stiffness function $k(t)$ for a single pair of teeth in one meshing period. In the meshing of the identical gear pair, the variation frequency of the stiffness is the same as the frequency of the inner excitation so that it can be represented as a Fourier series expansion:

$$\begin{aligned} k(t) &= k_m + \sum_{i=1}^{\infty}\left[a_i\cos(i\omega_h t) + b_i\sin(i\omega_h t)\right] \\ &= k_m + \sum_{i=1}^{\infty} k_i\cos(i\omega_h t) \end{aligned} \tag{3}$$

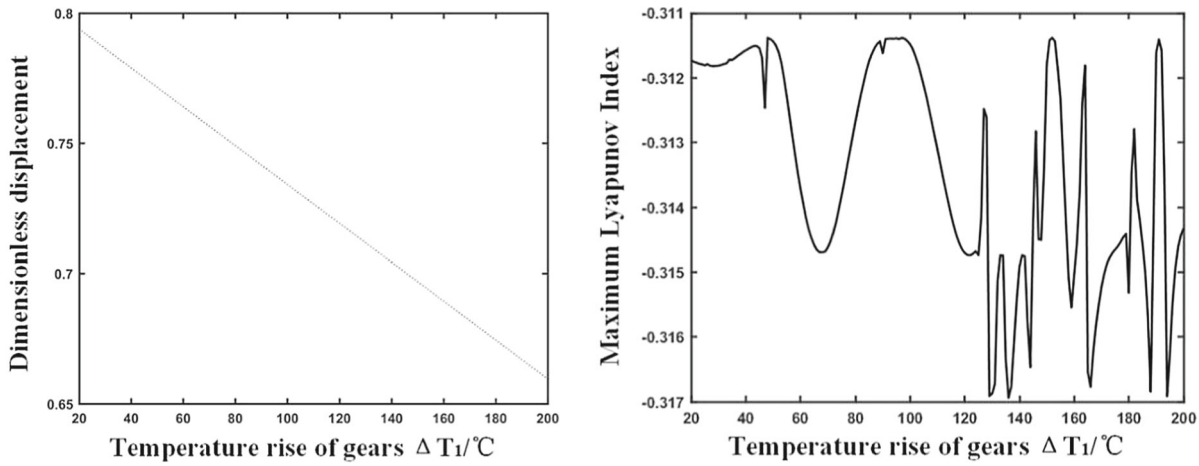

Fig. 4 **a** Bifurcation diagram of the gear system with gear temperature (s = 0.1) **b** Maximum Lyapunov Index Diagram

In the formula, k_{m} is the average meshing stiffness, $\sum_{i=1}^{\infty} k_i \cos(i\omega_h t)\ (i = 1, 2, 3 \cdots)$ is the harmonic component, ω_h is the gear meshing frequency.

If the first-order harmonic component of the stiffness is taken, the time-varying meshing stiffness is:

$$k(t) = k_m + k_a \cos(\overline{\omega}_h \bar{t}) \tag{4}$$

In the formula, k_a is the fluctuation amplitude of gear meshing stiffness.

2.2 Gear side clearance

The gear side clearance function is the nonlinear meshing force displacement function of the gear in the presence of side clearance [21], which is a segmented function. Assuming a side gap of 2b, the segmentation function $f(\overline{x}(\bar{t}))$ can be expressed as:

$$f(\overline{x}(\bar{t})) = \frac{\overline{f}(\overline{x}(\bar{t}))}{k_m} = \begin{cases} \overline{x}(\bar{t}) - b & \overline{x}(\bar{t}) > b \\ 0 & |\overline{x}(\bar{t})| < b \\ \overline{x}(\bar{t}) + b & \overline{x}(\bar{t}) < -b \end{cases} \tag{5}$$

If the gap is symmetrical, then $f(\overline{x}(\bar{t}))$ is shown in Fig. 2:

Changes in the parameters of the gear pair cause variations in the motion process of the gear, while changes in temperature cause changes in the tooth side clearance in response. For spur gears, the reduction in tooth side clearance due to temperature changes during gear operation Δb_1 is [22]:

$$\Delta b_1 = \Delta \mathrm{T}_1 \gamma_1 (1 + \Delta \mathrm{T}_1 \gamma_1) m\pi + [m \Delta \mathrm{T}_1 \gamma_1 (z_1 + z_2) \sin\alpha]/2 \tag{6}$$

where: z_1 and z_2 are the numbers of teeth of the main wheel and driven wheel, respectively; m is the gear modulus; α' is the angle of engagement after thermal deformation; $\alpha' = \arccos(a\cos\alpha/\alpha')$; $\Delta \mathrm{T}_1$ is the temperature rise of the gears; γ_1 is the coefficient of linear expansion of the gear.

Therefore, the tooth side clearance is redefined under the influence of temperature variation as:

$$2b' = 2b - \Delta b_1 \tag{7}$$

where: $2b'$ is the tooth side clearance considering the temperature change.

Then the tooth side clearance function including the temperature effect $f'(\overline{x}(\bar{t}))$ is:

$$f'(\bar{x}(\bar{t})) = \begin{cases} \bar{x}(\bar{t}) - b' & \bar{x}(\bar{t}) > b' \\ 0 & |\bar{x}(\bar{t})| < b' \\ \bar{x}(\bar{t}) + b' & \bar{x}(\bar{t}) < -b' \end{cases} \tag{8}$$

2.3 Engagement error and engagement damping

The transmission error of the gear static can be expressed in the Fourier series as [23]:

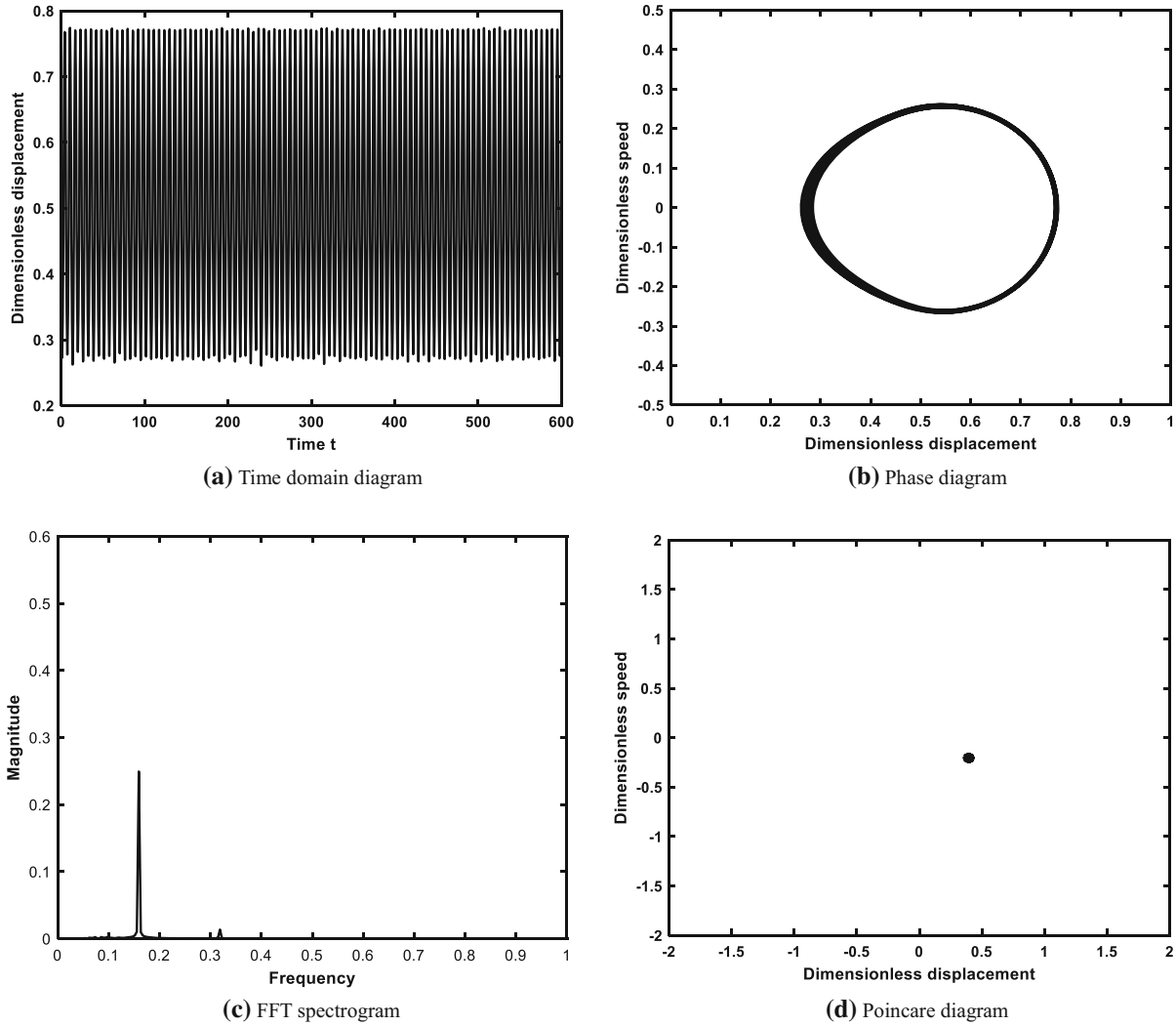

(a) Time domain diagram

(b) Phase diagram

(c) FFT spectrogram

(d) Poincare diagram

Fig. 5 Motion characteristics of the gear system at a temperature rise of 50 °C (s = 0.1)

$$e(\bar{t}) = e_m + \sum_{h=1}^{\infty} [e_{2h}\cos(n\omega_h t) + e_{2h+1}\sin(n\omega_h t)] \tag{9}$$

where e_{m} is the averaged meshing error, ω_h is the excitation frequency of the meshing error. Considering only the first order, taking $e_{\mathrm{m}} = 0$, the static engagement error expression can be reduced to:

$$e(\bar{t}) = e_a\cos(\omega_h t + \varphi_0) \tag{10}$$

where e_{a} is the error magnitude.

In the meshing line direction, the movements of the two gears are defined as x_1, x_2, and x_1 represent the movements of the driving wheel, x_2 represents follower wheel displacement. Obtains:

$$\begin{cases} x_1 = r_1\theta_1 \\ x_2 = r_2\theta_2 \end{cases} \tag{11}$$

The dynamic transmission error of the gear system is:

$$x_d(t) = x_1 - x_2 \tag{12}$$

Using $x(t)$ to express the integrated transmission error of the system, then $x(t)$ is the difference between the dynamic transfer error and the static transfer error. Then:

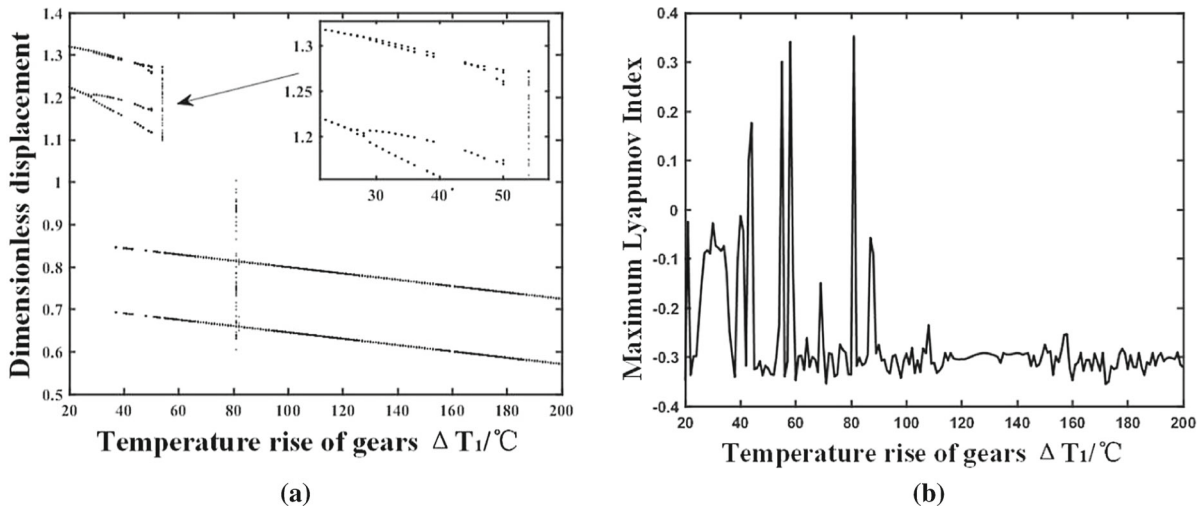

Fig. 6 **a** Bifurcation diagram of the gear system with gear temperature (s = 0.6) **b** Maximum Lyapunov Index Diagram

Table 1 Dynamic state of the gear system with the change of temperature rise ΔT_1

ΔT_1	$\Delta T_1 < 26$ °C	26 °C $< \Delta T_1 <$ 50 °C	50 °C $< \Delta T_1 <$ 80 °C	$\Delta T_1 = 80$ °C	80°C $< \Delta T_1 <$ 200 °C
Gear system dynamic state	Two times periodic	Four times periodic	Two times periodic	Chaotic state	Two times periodic

$$x(t) = x_1 - x_2 - e(\bar{t}) \tag{13}$$

The engagement damping is obtained by taking the empirical formula [24]:

$$c_h = 2\xi\sqrt{\frac{k_m I_1 I_2}{r_{b1}^2 I_1 + r_{b2}^2 I_2}} \tag{14}$$

where: r_{b1}, r_{b2} are the base circle radius of the master and follower wheels, respectively; I_1, I_2 are the rotational inertia of the driving and driven wheel, respectively; ξ is the damping ratio, usually takes the value of 0.03 $\sim$ 0.17.

2.4 Model establishment

The gear system has an overall mass concentration in the working process, so the concentrated mass method can be used to model the nonlinear dynamics of the gear system. The main method is to equate the gear system as a mass block with only mass and no consideration of elasticity and spring with only elasticity and no consideration of mass. It is assumed that the stiffness of the shaft in the gear system is large enough; the frictional influence of the bearing is not considered; and the direction of the force acts on the meshing line all the time. Then the kinetic model of a pair of cylindrical gear pairs is presented in Fig. 3.

In the figure: r_{b1} and r_{b2} are the radii of the base circle of the master and driven wheel, respectively; T_1 and T_2 are the torques applied to the main driven wheel, respectively; θ_1 and θ_2 are the torsional vibration displacement of the two gears, respectively; $e(t)$ is the static transmission error of gear meshing; c_h is the damping coefficient in gear meshing; $k(t)$ is the time-varying meshing stiffness of the gear.

According to the dynamics model of the gear system shown in the figure, the differential equations of motion of the system model can be obtained from Newton's laws of mechanics as:

$$\begin{cases} \overline{T}_1 = I_1\ddot{\theta}_1 + r_{b1}c_h[r_{b1}\dot{\theta}_1 - r_{b2}\dot{\theta}_2 - \dot{e}(\bar{t})] + k(\bar{t})r_{b1}\overline{f}(r_{b1}\theta_1 - r_{b2}\theta_2 - e(\bar{t})) \\ -\overline{T}_2 = I_2\ddot{\theta}_2 - r_{b2}c_h[r_{b1}\dot{\theta}_1 - r_{b2}\dot{\theta}_2 - \dot{e}(\bar{t})] - k(\bar{t})r_{b2}\overline{f}(r_{b1}\theta_1 - r_{b2}\theta_2 - e(\bar{t})) \end{cases} \tag{15}$$

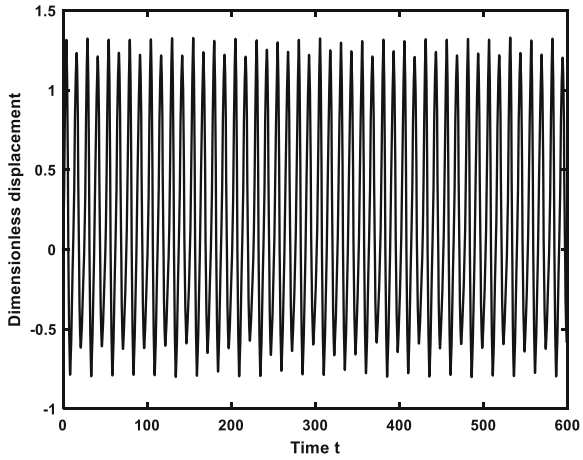

(a) Time domain diagram

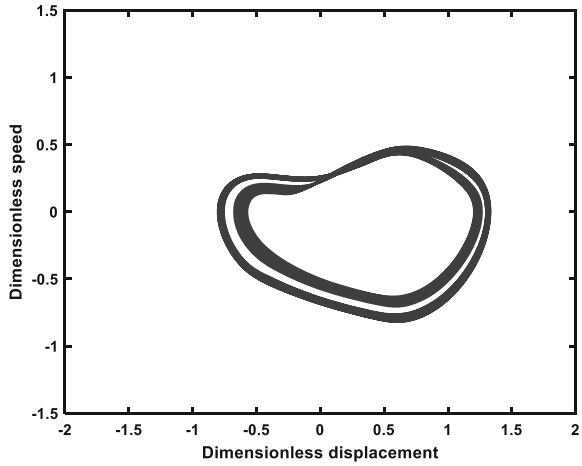

(b) Phase diagram

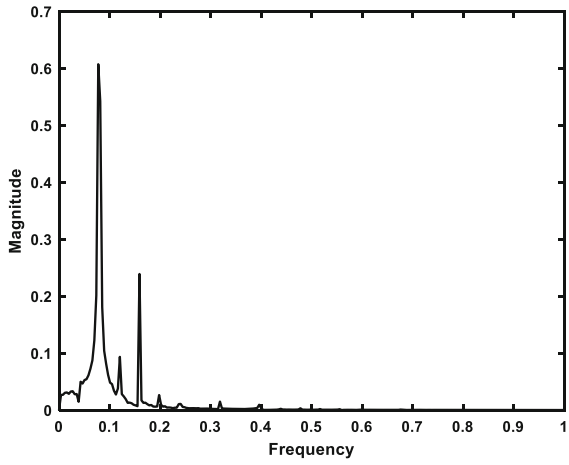

(c) FFT spectrogram

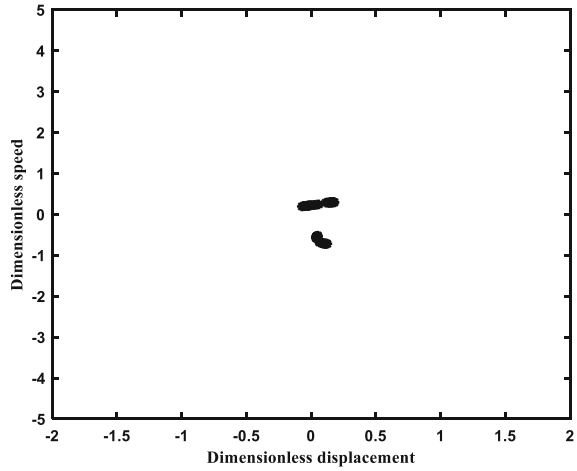

(d) Poincare diagram

Fig. 7 Motion characteristics of the gear system at a temperature rise of 20 °C (s = 0.6)

where: $\overline{T_1}$ and $\overline{T_2}$ are the external moments acting on the master and driven gears; I_1 and I_2 are the rotational inertia of the master and driven gears.

Dividing both ends of the first equation in Eq. (15) by r_{b1} and both ends of the second equation by r_{b2} at the same time:

$$\begin{cases} \bar{T}_1/r_{b1} = (I_1/r_{b1}^2)r_{b1}\ddot{\theta}_1 + c_h[r_{b1}\dot{\theta}_1 - r_{b2}\dot{\theta}_2 - \dot{e}(\bar{t})] \\ \qquad\qquad + k(\bar{t})\bar{f}(r_{b1}\theta_1 - r_{b2}\theta_2 - e(\bar{t})) \\ -\bar{T}_2/r_{b2} = (I_2/r_{b2}^2)r_{b2}\ddot{\theta}_2 - c_h[r_{b1}\dot{\theta}_1 - r_{b2}\dot{\theta}_2 - \dot{e}(\bar{t})] \\ \qquad\qquad - k(\bar{t})\bar{f}(r_{b1}\theta_1 - r_{b2}\theta_2 - e(\bar{t})) \end{cases} \tag{16}$$

Order:

$$\begin{cases} m_1 = I_1/r_{b1}^2,\ m_2 = I_2/r_{b2}^2 \\ \overline{F}_1 = \overline{T}_1/r_{b1},\ \overline{F}_2 = \overline{T}_2/r_{b2} \end{cases} \tag{17}$$

A transformation of Eq. (16) yields:

$$\begin{cases} \overline{F}_1 = m_1\ddot{x}_1 + c_h[\dot{x}_1 - \dot{x}_2 - \dot{e}(\bar{t})] + k(\bar{t})\bar{f}(x_1 - x_2 - e(\bar{t})) \\ -\overline{F}_2 = m_2\ddot{x}_2 - c_h[\dot{x}_1 - \dot{x}_2 - \dot{e}(\bar{t})] - k(\bar{t})\bar{f}(x_1 - x_2 - e(\bar{t})) \end{cases} \tag{18}$$

where:m_1, m_2 are the equivalent masses of the master and follower gears, respectively;$\overline{F}_1$, $\overline{F}_2$ are the circumferential forces along the meshing line of the master and driven gears, respectively.

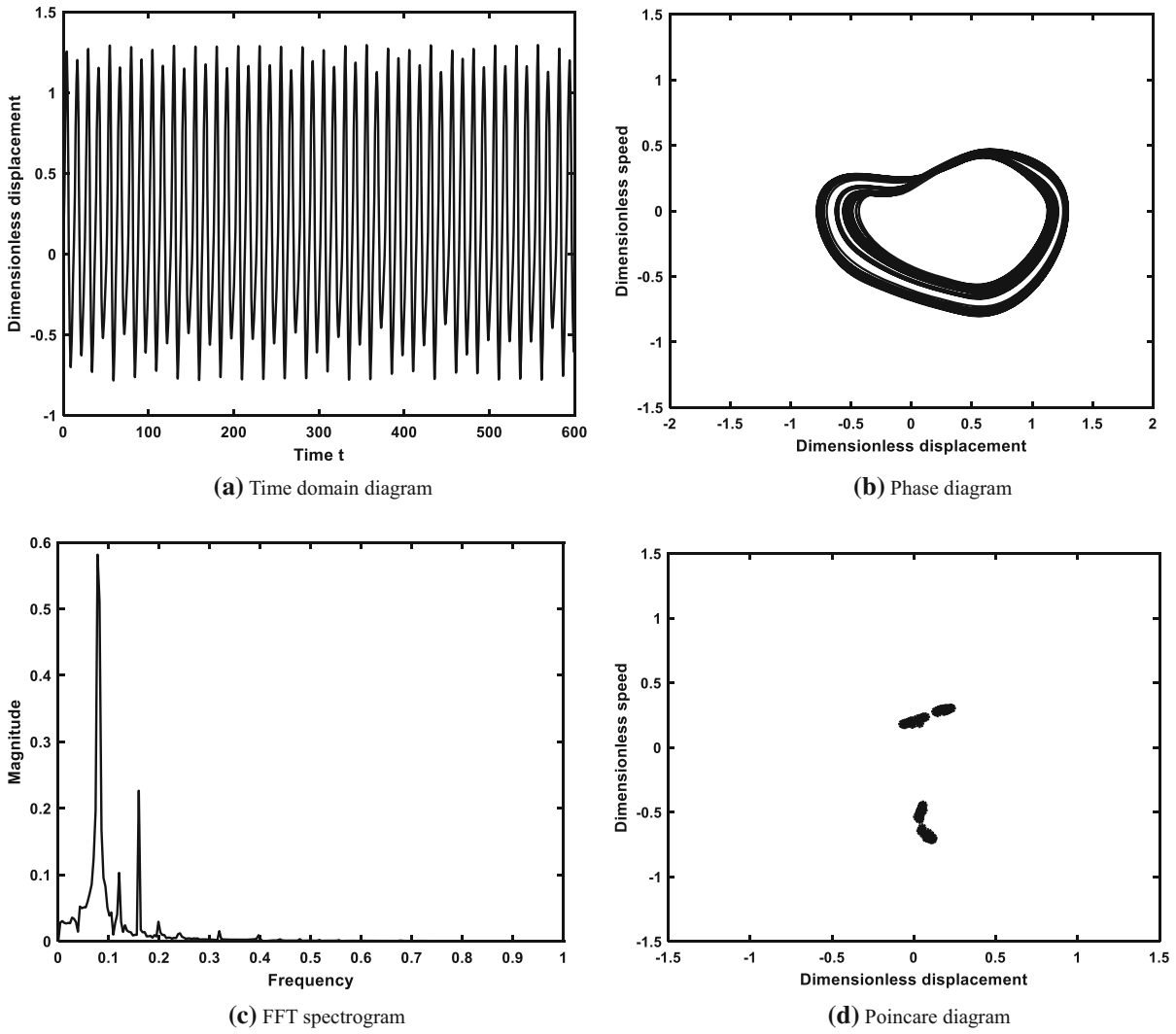

(a) Time domain diagram

(b) Phase diagram

(c) FFT spectrogram

(d) Poincare diagram

Fig. 8 Motion characteristics of the gear system at a temperature rise of 42 °C (s = 0.6)

Multiplying the first equation in Eq. (18) by m_2/m_1 and subtracting the second equation yields:

$$\begin{aligned} m_2/m_1 \cdot \overline{F}_1 + \overline{F}_2 =& m_2(\ddot{x}_1 - \ddot{x}_2 - \ddot{e}(\bar{t}) + \ddot{e}(\bar{t}) \\ &+ (m_1 + m_2)/m_1 \cdot \{c_h[\dot{x}_1 - \dot{x}_2 - \dot{e}(\bar{t})] \\ &+ k(\bar{t})\overline{f}(x_1 - x_2 - e(\bar{t}))\} \end{aligned} \tag{19}$$

Then multiply both ends of Eq. (19) by $\frac{m_1}{m_1+m_2}$ at the same time, and make $m_e = \frac{m_1 m_2}{m_1+m_2}$, then the analytical model for the dynamics of the gear pair expressed in Eq. (15) can be adapted as:

$$m_e\ddot{\overline{x}} + c_h\dot{\overline{x}} + k(\bar{t})f(\overline{x}) = \frac{m_e}{m_1}\overline{F}_1 + \frac{m_e}{m_2}\overline{F}_2 - m_e\ddot{e}(\bar{t}) \tag{20}$$

Order:

$$\overline{F}_m = \frac{m_e}{m_1}\overline{F}_1 + \frac{m_e}{m_2}\overline{F}_2,\ \overline{F}_h = -m_e\ddot{e}(\bar{t}), \tag{21}$$

Then:

$$m_e\ddot{\overline{x}} + c_h\dot{\overline{x}} + k(\bar{t})f(\overline{x}) = \overline{F}_m + \overline{F}_h \tag{22}$$

where m_e is the equivalence mass of the gear pair, $\overline{F}_m$ is the outer excitation of the gear system, $\overline{F}_h$ is the internal excitation of the gear system. In a system of gears, both its external and internal excitation can be represented as a periodic function of time, then:

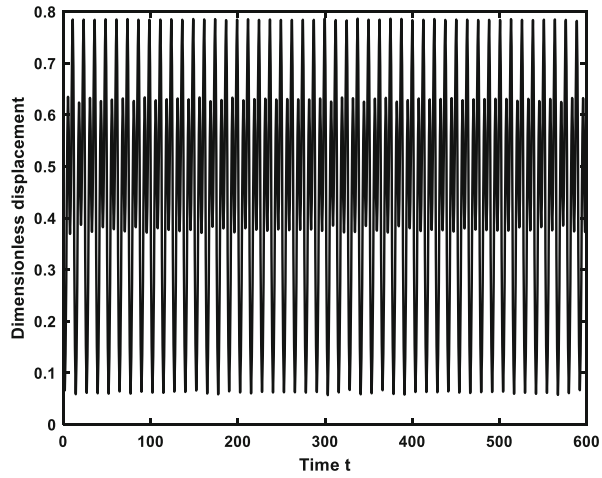

(a) Time domain diagram

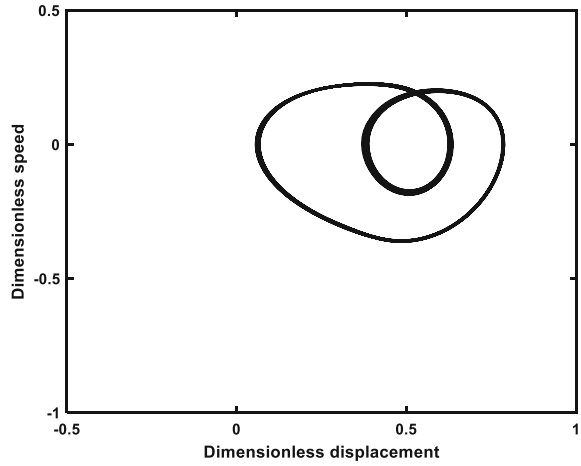

(b) Phase diagram

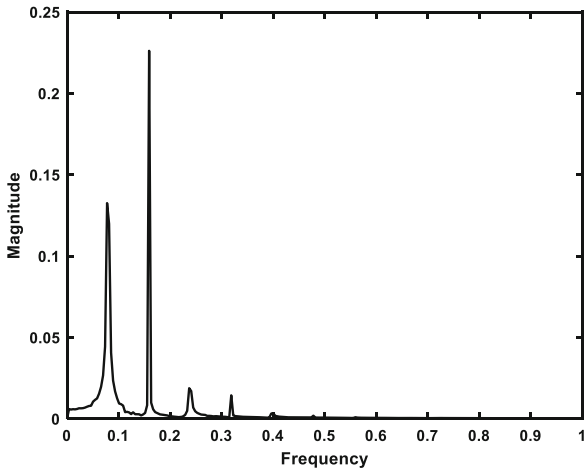

(c) FFT spectrogram

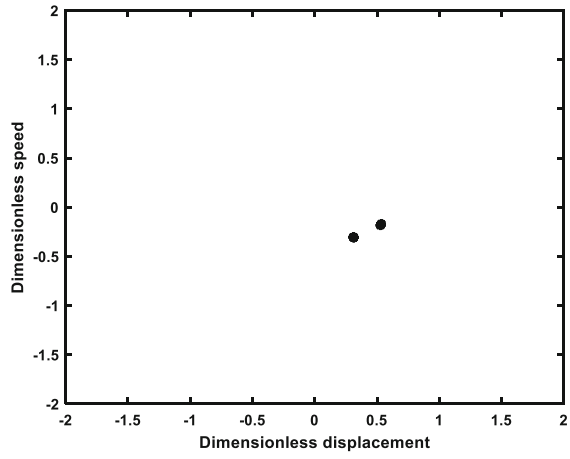

(d) Poincare diagram

Fig. 9 Motion characteristics of the gear system at a temperature rise of 120 °C (s = 0.6)

$$\overline{F}_m(\overline{t}) = \overline{F}_{m0} + \tilde{F}_m \sin(\overline{\omega}_m \overline{t} + \phi_m) \tag{23}$$

$$e(\overline{t}) = \tilde{e} \sin(\overline{\omega}_h \overline{t} + \phi_h) \tag{24}$$

Substituting Eqs. (4), (23) and (24) into Eq. (20) yields:

$$\begin{aligned} m_e \ddot{\overline{x}} + c_h \dot{\overline{x}} + (k_m + k_a \cos(\overline{\omega}_h \overline{t})) f(\overline{x}) \\ = \overline{F}_m + m_e \tilde{e} \overline{\omega}_h^2 \sin(\overline{\omega}_h \overline{t} + \phi_h) \end{aligned} \tag{25}$$

To facilitate the computational study of the dynamics of the gear system, the dynamics equations need to be dimensionless. Define the quantization time as $t = \omega_0 \overline{t}$, ω_0 is the intrinsic frequency of the gear dynamics model, the solution formula is $\omega_0 = \sqrt{\frac{k_m}{m_e}}$. Introducing displacement nominal scales b_c, then the other variables can be defined by $\overline{t}$ and b_c, Assuming constant average meshing stiffness, $x = \overline{x}/b_c$ [25]. Order:

$$\begin{aligned} \overline{\omega}_h = \frac{\omega_h}{\omega_0}, \overline{\omega}_m = \frac{\omega_m}{\omega_0}, F_m = \frac{\overline{F}_m}{b_c m_e \omega_0^2}, F_h = \frac{\tilde{e}}{b_c m_e \omega_0^2}, \xi \\ = \frac{c_h}{2 m_e \omega_0}, s = \frac{k_a}{k_m} \end{aligned} \tag{26}$$

This leads to the dimensionless analytical model of the nonlinear dynamics of the gear system considering the temperature effect as:

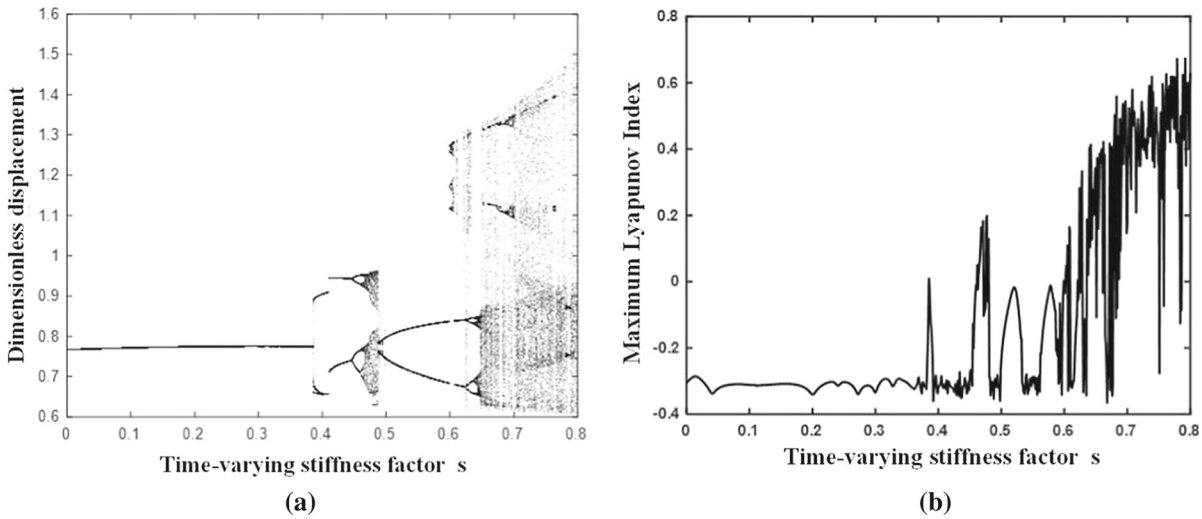

Fig. 10 **a** Bifurcation diagram of the gear system for the variation of the readily variable stiffness coefficient s (ΔT_1 = 50 °C) **b** Maximum Lyapunov Index Diagram

$$\ddot{x}(t) + 2\xi\dot{x}(t) + [1 + s\cos\omega_h t]f'(x(t)) = F_m + F_h\omega_h^2\sin(\omega_h t + \phi_h) \quad (27)$$

where, ξ is the damping factor, x(t) is the transfer error of dimensionless processing, s is the ratio of the engagement rigidity fluctuation to the average component, which is the time-varying rigidity factor, F_{m} is the average load, $F_h\omega_h^2\sin(\omega_h t + \phi_h)$ is the internal load, $f'(x(t))$ is the dimensionless nonlinear displacement function considering the temperature response.

3 Analysis of nonlinear dynamics

According to the results after normalization of the equation magnitudes, it can be seen that the dynamics model of the gear is a multivariate nonlinear system, and it is difficult to analyze the influence of each factor on the stability of the system simultaneously. The literature [26] used the Sobol's method of global sensitivity analysis based on variance to investigate the influence of various factors on the dynamic properties of the system, and the results indicated that the tooth side clearance has an enormous influence on the system motion characteristics. The literature [27] used the incremental harmonic balance method (IHBM) to analyze the influence of dynamic tooth gap, time-varying rigidity, excitation force amplitude and damping ratio on the dynamic properties of the gear pair system. The findings showed that the time-varying meshing rigidity, damping ratio and tooth gap have the most significant effects on the nonlinear characteristics of the system.

The gear system analyzed in this paper is an involute spur gear system, and the dynamic properties of the gear system will be investigated from three aspects: tooth side clearance, time-varying meshing rigidity and meshing damping ratio. The following system parameters were selected [28]: average load F_{m} = 0.1, damping ratio ξ = 0.05, error magnitude F_{h} = 0.05, initial tooth side clearance b = 0.5, dimensionless frequency ω_h = 1.

3.1 The influence of temperature on system characteristics

The working environment of the gear system is complex and there are many external influencing factors, for example, when the gear is operating at high speed, the working temperature of the gear system will increase due to power loss. In addition, gearboxes are designed for ambient temperature conditions, but the ambient temperature varies from region to region, so it is necessary to analyze the effect of temperature changes on the gear system.

The bifurcation diagram and the maximum Lyapunov index diagram are reliable tool diagrams for observing the dynamic response of the system. When the time-varying stiffness coefficient s is small, keep s = 0.1 constant, and the bifurcation diagram and the

Table 2 Dynamical state of the gear system with the change of Time-varying stiffness coefficient s

s	$0 < s < 0.386$	$0.386 < s < 0.4$	$0.4 < s < 0.464$	$0.464 < s < 0.47$	$0.47 < s < 0.5$	$0.5 < s < 0.6$	$0.6 < s < 0.8$
Gear system dynamic state	Single times periodic	Three times periodic	Two times periodic	Four times periodic	Chaotic state	Two times periodic	Chaotic state

maximum Lyapunov index diagram of the gear system when the temperature rise is varied from 20 to 200 °C are shown in Fig. 4.

As shown in the figure, when the time-varying stiffness coefficient is small, the kinematic characteristics of the gear system are relatively stable with the constant change of temperature, and it has been maintained in a state of cyclic motion, and its maximum Lyapunov index in general has been kept in a negative state. The temperature rise is now taken as 50 °C. The simulation obtains the time domain diagram, phase diagram, spectrum diagram and Poincaré cross section of the gear system, as shown in Fig. 5. As can be seen from Fig. 5, when the temperature rise is 50 °C, the time domain diagram of the gear system is a periodic curve with regular peaks, the phase diagram is a single closed loop, the spectrum diagram shows an isolated peak straight line, and the Poincaré cross-sectional diagram aggregates to a single point, indicating that the system is in a stable single-fold periodic motion. The results show that when the time-varying stiffness coefficient is small, the temperature has less influence on the system characteristics. The gear system keeps a single-fold cycle motion with the change of gear temperature rise.

When the time-varying stiffness coefficient s is large, $s = 0.6$ is taken, and other parameters of the system are kept constant to obtain the bifurcation diagram and the maximum Lyapunov index diagram of the gear system when the gear temperature rise varies from 20 to 200 °C, as shown in Fig. 6. The dynamic state of the gear system with the change of temperature rise is shown in Table 1.

As shown in Fig. 6, for a time-varying stiffness factor of $s = 0.6$, the gear system exhibits two times the proposed periodic motion when the gear temperature rises $\Delta T_1 < 26$ °C. As shown in Fig. 7, when the temperature rise $\Delta T_1 = 20$ °C, the time domain diagram presents a periodic curve with regular peaks, the phase diagram is a closed curve band with a certain width, and the Poincare diagram is composed of two point sets, so the system is in two times anthropomorphic periodic motion state at this time. In Fig. 6, with the increase of gear temperature rise, the gear system first bifurcates from two times the proposed periodic motion to four times the proposed periodic motion, and the time domain diagram, phase diagram and Poincare section diagram at $\Delta T_1 = 42$ °C are shown in Fig. 8, The time domain diagram shows a periodic

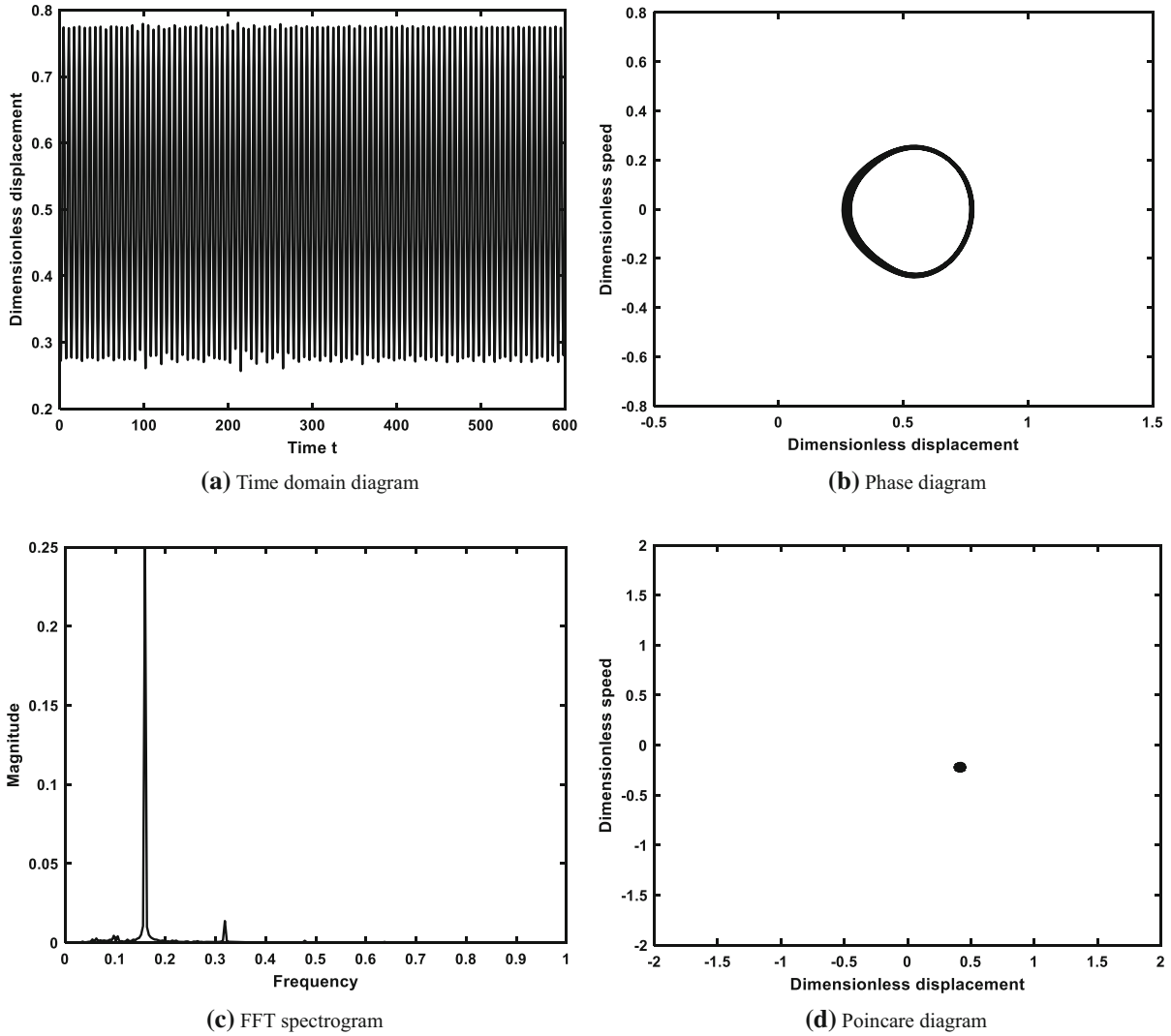

(a) Time domain diagram

(b) Phase diagram

(c) FFT spectrogram

(d) Poincare diagram

Fig. 11 Dynamic characteristics of the gear system with time-varying stiffness coefficient $s = 0.2$ ($\Delta T_1 = 50$ °C)

curve with regular peaks, the phase diagram is a closed curve band, and the Poincare diagram consists of four point sets, so the system is in four times the proposed periodic motion at this time; The system then enters into a two-fold periodic motion, Fig. 9 shows the time domain diagram and phase diagram of the gear system at $\Delta T_1 = 120$ °C, the time domain diagram shows a periodic curve with regular peaks, and the phase diagram is a closed curve band, while there are only two points on the Poincare section diagram, so the system is in a twofold periodic motion at this time. As can be seen, the variation of the system motion characteristics with gear temperature rise obtained in Figs. 7, 8, 9 remains consistent with the results presented in the bifurcation diagram and the maximum Lyapunov index diagram shown in Fig. 6.

The results show that the temperature variation has a greater impact on the motion characteristics of the gear system when the time-varying stiffness factor is significant, and the gear system undergoes a " two times—four times—two times" cyclic motion variation with the change of temperature rise.

From the above analysis, it can be obtained that the change of gear temperature has different effects on the system motion characteristics under different time-varying stiffness coefficients. Therefore, for some gear systems with special working conditions, reasonable

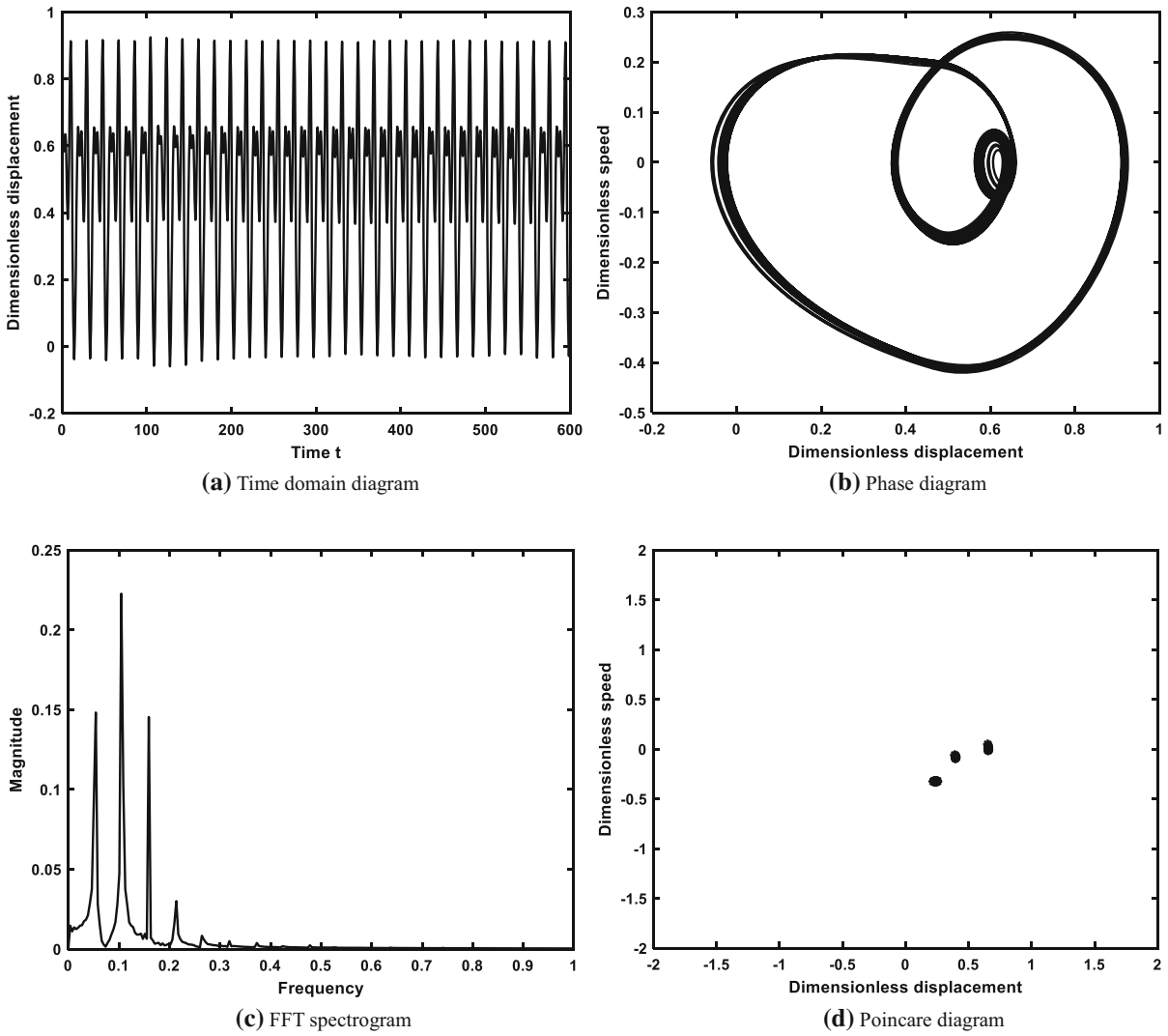

(a) Time domain diagram

(b) Phase diagram

(c) FFT spectrogram

(d) Poincare diagram

Fig. 12 Dynamic characteristics of the gear system with time-varying stiffness coefficient $s = 0.39$ ($\Delta T_1 = 50$ °C)

gear system parameters are very important for the system motion characteristics.

3.2 Effect of time-varying stiffness coefficients on system characteristics

The time-varying stiffness coefficient s reflects the variation of the meshing stiffness with time and is one of the internal excitation parameters affecting the dynamic characteristics of the gear system. The dynamic characteristics of the gear system are analyzed with the time-varying stiffness coefficient s as the control parameter, taking the gear temperature rise as 50 °C and other parameters of the system as constant. Figure 10 shows the bifurcation diagram and the maximum Lyapunov exponent for the variation of the readily variable stiffness coefficient s. The dynamical states of the gear system with the change of the variable stiffness coefficient s are shown in Table 2. Figures 11, 12, 13, 14, 15 show the phase diagram, Poincare mapping and time domain spectrum of the system when the time-varying stiffness coefficient takes different values, which can explain the dynamics of the gear system in more detail when the time-varying stiffness coefficient is varied.

As shown in Fig. 10, the gear system exhibits different motion states when the time-varying stiffness factor s is varied. As the time-varying stiffness

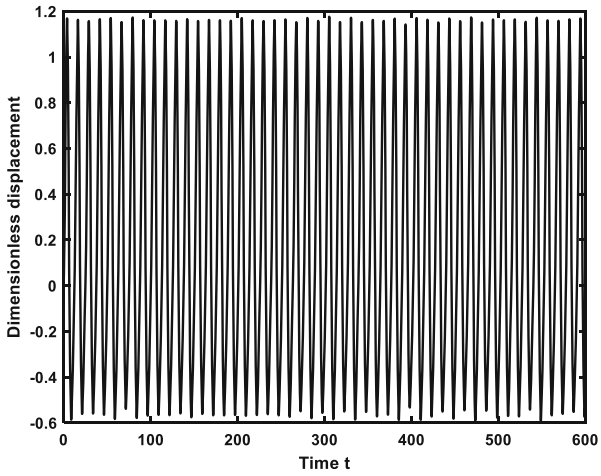

(a) Time domain diagram

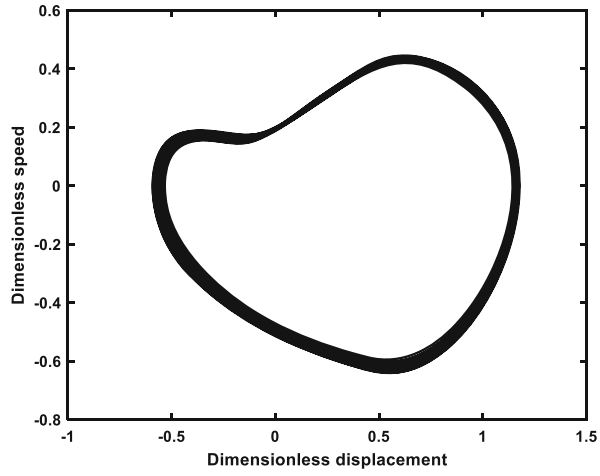

(b) Phase diagram

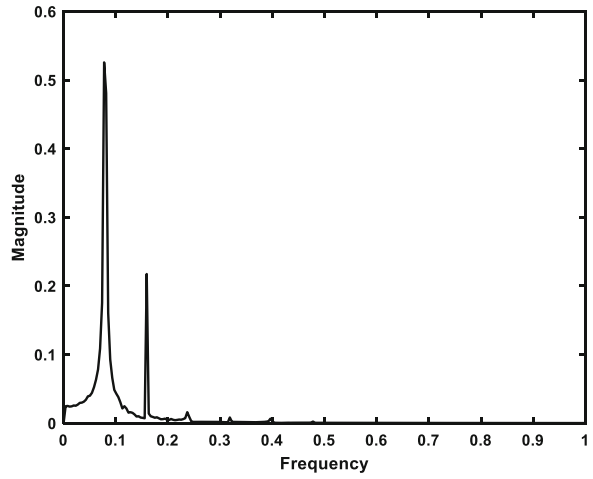

(c) FFT spectrogram

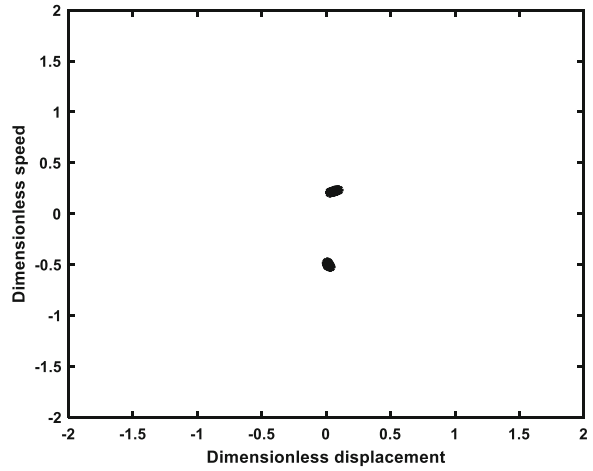

(d) Poincare diagram

Fig. 13 Dynamic characteristics of the gear system with time-varying stiffness coefficient $s = 0.45$ ($\Delta T_1 = 50$ °C)

coefficient s increases from 0 to 0.386, the gear system is in single-cycle motion, when its maximum Lyapunov index is less than 0; Fig. 11 shows the time domain diagram, phase diagram and Poincare section diagram at $s = 0.2$. The time domain diagram presents a periodic curve with regular peaks, the phase diagram is a closed curve, and the Poincare section diagram shows a point, indicating that the system is in a single period motion at this time. When $s > 0.386$, the gear system first enters a short period three motion, then becomes a period two motion, and then changes from a period two to a period four motion, and the maximum Lyapunov exponent goes through a "negative-zero-negative–positive" change; Fig. 12 shows the kinematic characteristics at $s = 0.39$, the time domain diagram is a periodic curve with regular peaks, the phase diagram has a three-loop winding closed curve, and the Poincare section diagram also has three discrete points, indicating that the system is in a period three motion at this time. The kinematic characteristics at $s = 0.45$ are shown in Fig. 13, the phase diagram is a closed curve with a certain width, and the Poincare cross section consists of two point sets, proving that the system is in a two-fold proposed periodic motion at this time. According to the bifurcation diagram, when the time-varying stiffness coefficient $s > 0.464$ increases further, the gear system first enters the chaotic motion state, then enters the

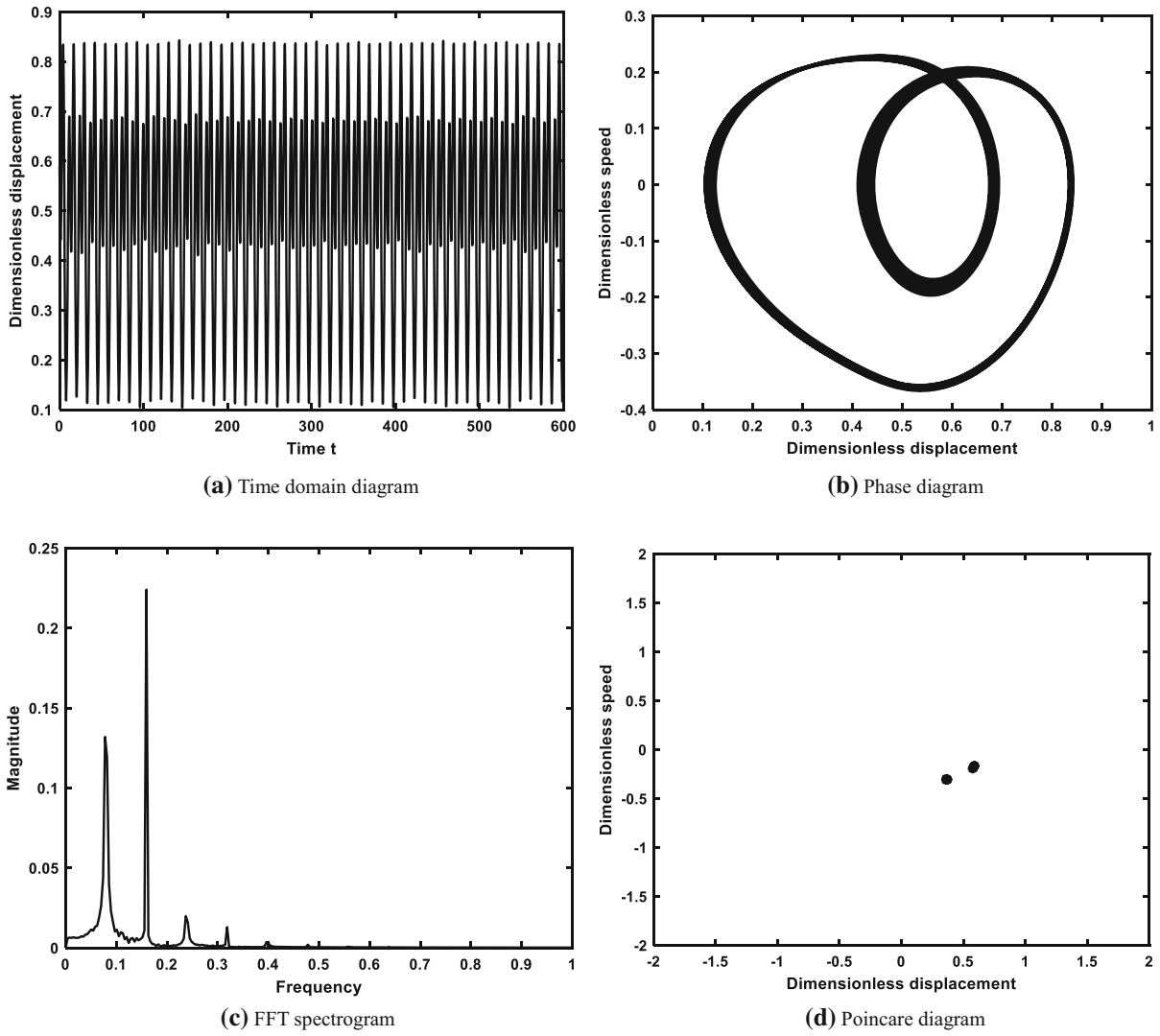

(a) Time domain diagram

(b) Phase diagram

(c) FFT spectrogram

(d) Poincare diagram

Fig. 14 Dynamic characteristics of the gear system with time-varying stiffness coefficient $s = 0.56$ ($\Delta T_1 = 50$ °C)

two-fold period motion, and then enters the chaotic state again, and its maximum Lyapunov exponent goes through the change of "positive-zero-negative–positive." When $s = 0.56$, the kinematic characteristics of the gear system are shown in Fig. 14, the time domain diagram is a periodic curve with regular peaks, the phase diagram has a two-loop winding closed curve, and the Poincare section diagram has two point sets, so the system is in a two-fold periodic motion at this time. The time-varying stiffness coefficient s continues to increase, and when $s = 0.75$, the system motion characteristic diagram is shown in Fig. 15, the time domain diagram is a curve without obvious periodicity, the phase diagram does not repeat and fills a certain closed area, and the Poincare section diagram consists of patches of dense points, so the system enters a complex chaotic motion phase.

The results show that the time-varying stiffness coefficient has a significant influence on the system characteristics. With the change of the time-varying stiffness coefficient, the gear system has the motion states of single-cycle, multi-cycle and chaotic motion. When the gear system is in a chaotic state, the degree of collision of gears becomes violent, and the long-term chaotic motion will aggravate the gear wear and reduce the gear life, so the appropriate time-varying stiffness coefficient should be selected to avoid entering the chaotic state when working.

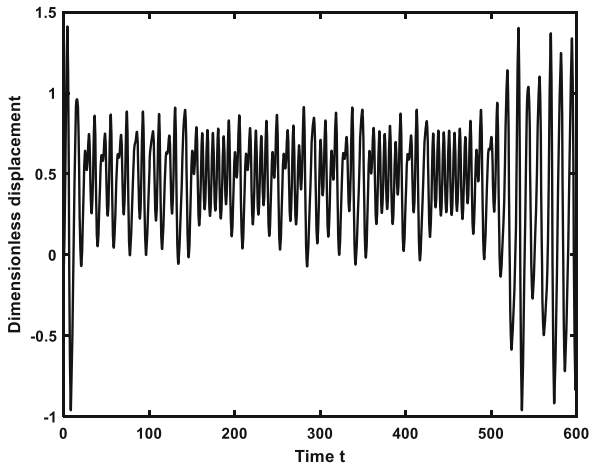

(a) Time domain diagram

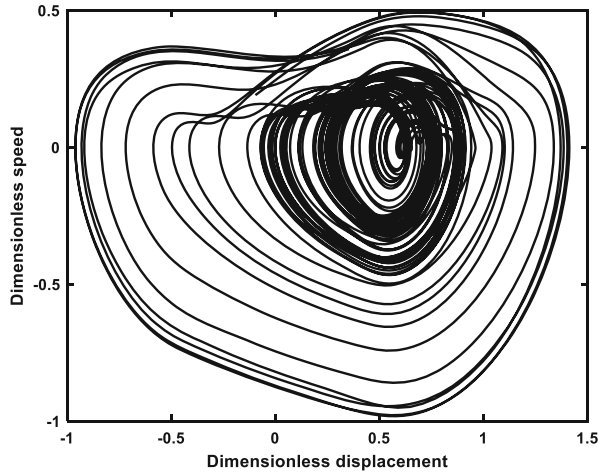

(b) Phase diagram

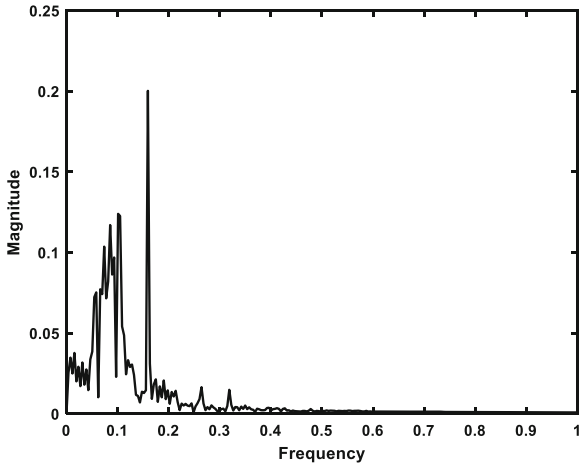

(c) FFT spectrogram

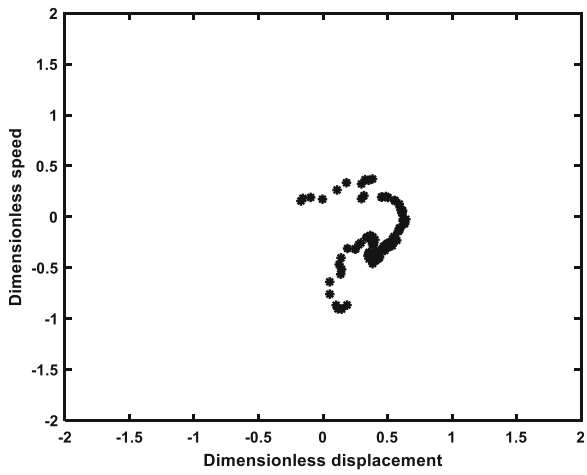

(d) Poincare diagram

Fig. 15 Dynamic characteristics of the gear system with time-varying stiffness coefficient $s = 0.75$ ($\Delta T_1 = 50$ °C)

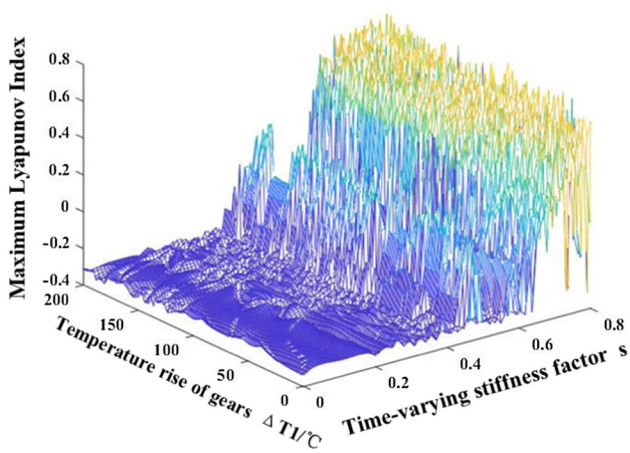

Fig. 16 Plot of the maximum Lyapunov index of the system for simultaneous changes in temperature and meshing stiffness coefficient

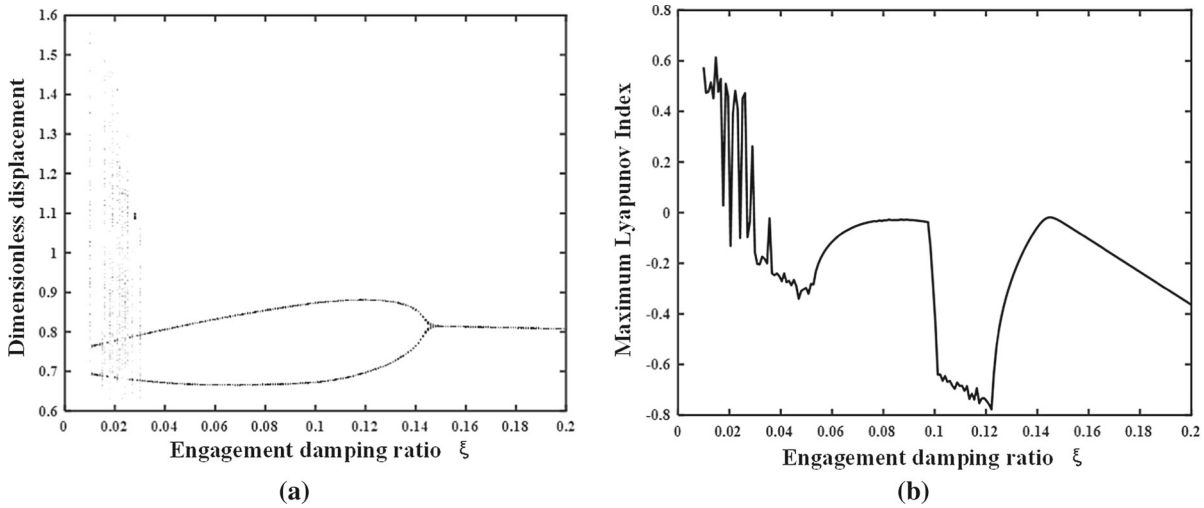

Fig. 17 **a** Bifurcation diagram of the gear system with the variation of the meshing damping ratio (ΔT_1 = 50 °C) **b** Maximum Lyapunov Index Diagram

Table 3 Dynamic state of the gear system with the change of meshing damping ratio ξ

ξ	$\xi < 0.03$	$0.03 < \xi < 0.148$	$\xi > 0.148$
Gear system dynamic state	Chaotic state	Two times periodic	Single times periodic

Figure 16 shows the maximum Lyapunov index diagram of the gear system for simultaneous changes in temperature and stiffness coefficients to reflect the bifurcation characteristics of the gear system. From Fig. 16, it can be seen that when the time-varying rigidity factor $s < 0.4$, the maximum Lyapunov index of the system has remained negative with the change of temperature, indicating that the gear system has been in a stable state of motion. And when the time-varying stiffness coefficient $s > 0.4$, the maximum Lyapunov index of the system varies with temperature, indicating that the gear system is in different states of motion at different temperatures. The results show that when the value of the time-varying stiffness coefficient of the gear system is small, the effect of temperature change on the motion state of the system is smaller. With the increase of the time-varying stiffness coefficient, the effect of temperature change on the system motion state is gradually significant.

3.3 Effect of the change of meshing damping on the dynamic characteristics of the system

Damping can reduce the vibration of gear systems by dissipating energy during transmission. The dynamic properties of the gear system are studied by taking the gear temperature rise as 50 °C and other parameters of the system as constant, and the mesh damping ratio ξ as the control parameter. Figure 17 shows the bifurcation chart and the maximum Lyapunov index of the gear system with the variation of the mesh damping ratio ξ. The dynamical states of the gear system with the change of the meshing damping ratio ξ are shown in Table 3.

From the bifurcation diagram shown in Fig. 17, the gear system is in a complex chaotic motion when the meshing damping ratio is taken as $\xi < 0.03$. When the meshing damping ratio rise to a value of $0.03 < \xi < 0.148$, the gear system is in twice the periodic motion. When the damping ratio rises to a value $\xi > 0.148$, the system is in a stable single-cycle motion. In the Maximum Lyapunov Exponential chart, the exponential goes through a "positive-zero-

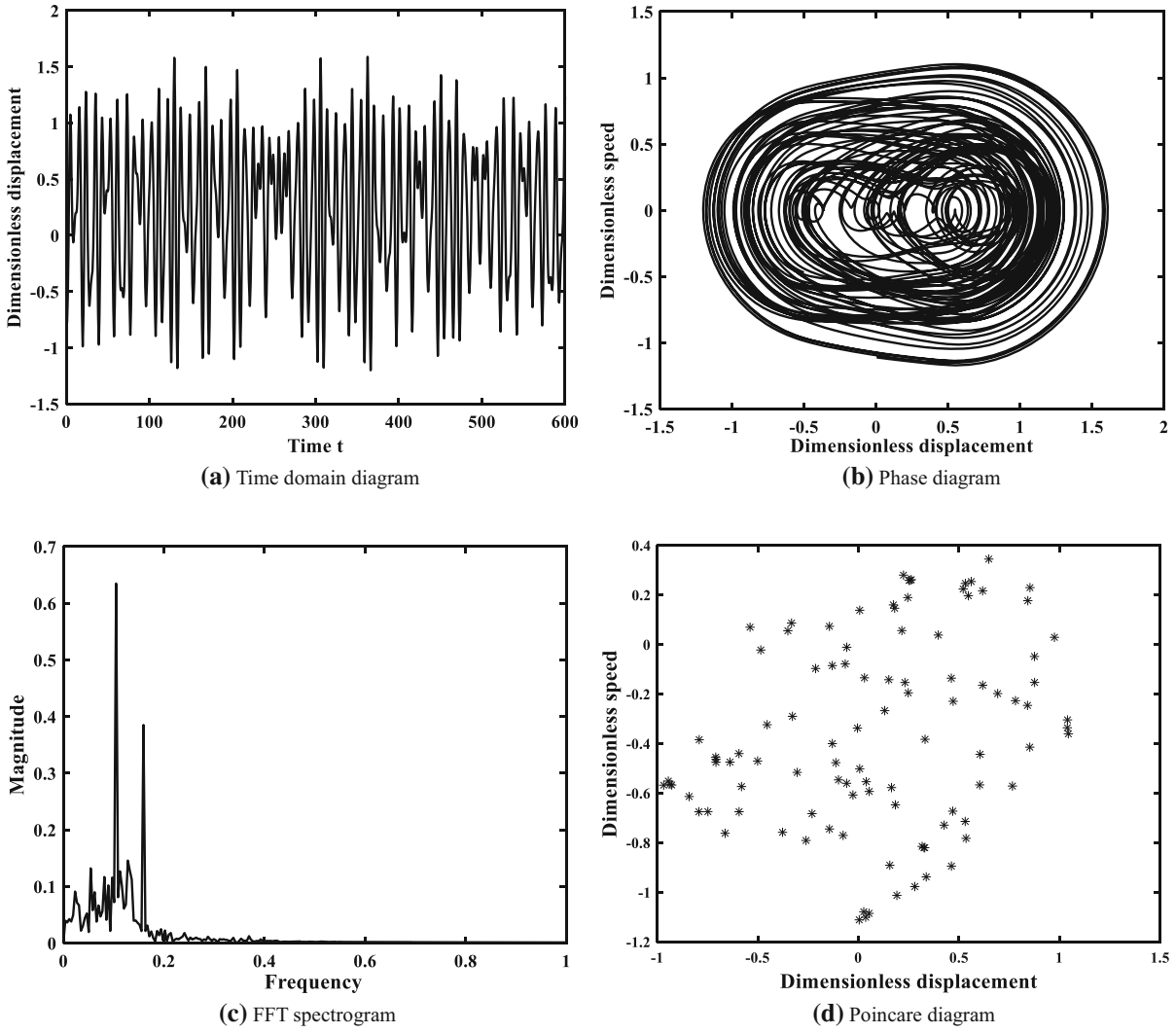

(a) Time domain diagram **(b)** Phase diagram

(c) FFT spectrogram **(d)** Poincare diagram

Fig. 18 Dynamic characteristics of the gear system with the mesh damping ratio $\xi = 0.01$ ($\Delta T_1 = 50$ °C)

negative" change, which is consistent with the variation of the movement state presented in the bifurcation chart. Figure 18 shows the time domain plot, phase diagram, FFT spectrum and Poincare cross section of the gear system when the mesh damping ratio takes different values.

As shown in Fig. 18, when $\xi = 0.01$, the time domain diagram of the gear system is a non-periodic curve, the phase plane graph does not duplicate and covers a closed area, the FFT diagram is a consecutive frequency band, and the Poincare section graph consists of pieces of dense points, therefore, the system behaves as a complicated chaotic movement at this point. As shown in Fig. 19, when $\xi = 0.08$, the time domain diagram is periodic, the phase plane graph is a closed curve band, and the FFT graph is discrete, so the motion characteristic of the system is periodic motion, and because the Poincare cross-section diagram contains two points, the system is two times periodic motion at this time. As shown in Fig. 20, when $\xi = 0.18$, the time domain diagram of the system has a certain periodicity, the phase plane diagram is a closed band of curves, the FFT graph is discrete, and the Poincare graph is constituted by only one point, therefore, the system shows a steady and regular single-fold periodic movement at this point.

The results indicate that with the increase of the mesh damping ratio, the motion state of the gear

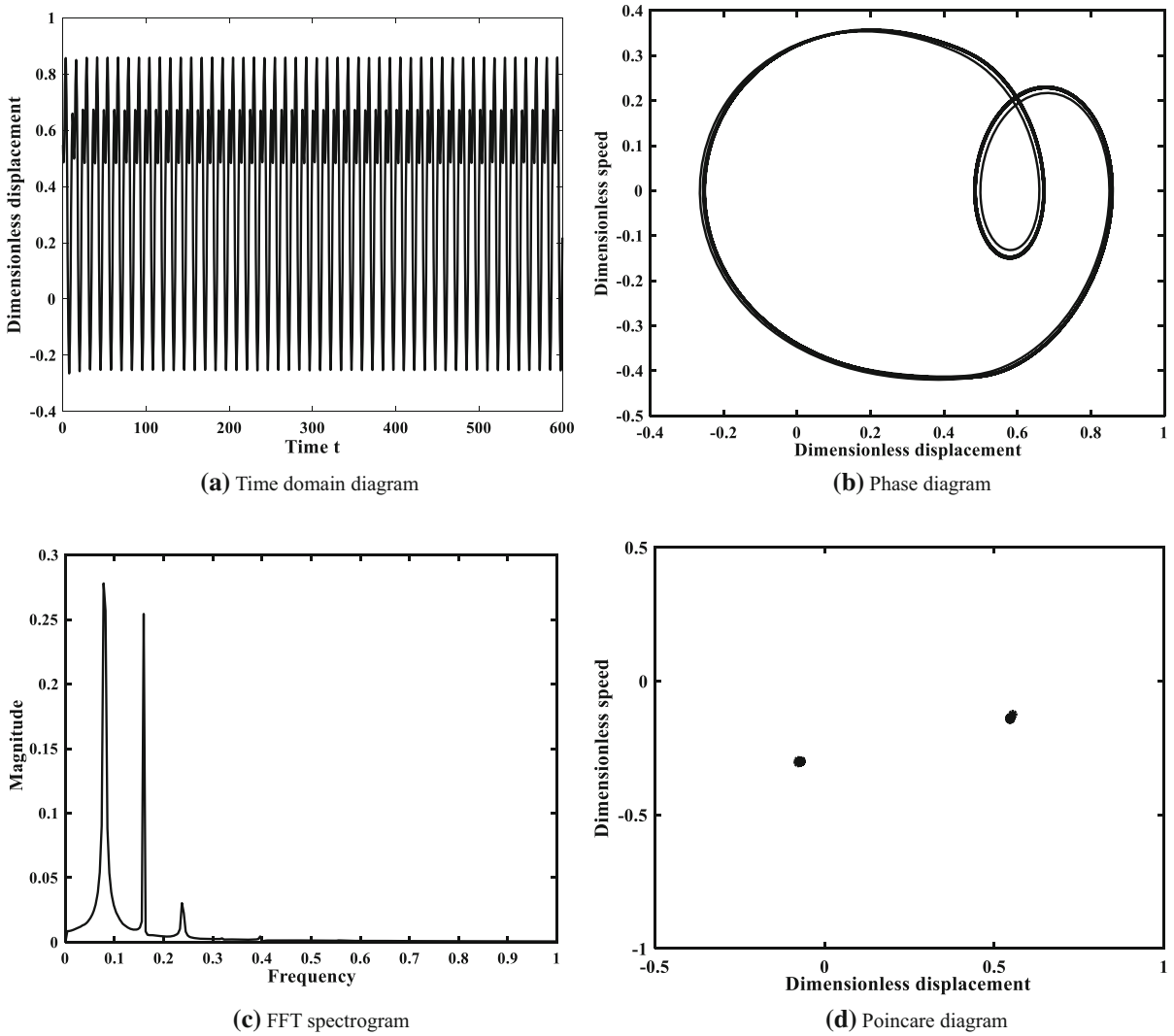

(a) Time domain diagram

(b) Phase diagram

(c) FFT spectrogram

(d) Poincare diagram

Fig. 19 Dynamic characteristics of the gear system with the mesh damping ratio $\xi = 0.08(\Delta T_1 = 50\ ^\circ C)$

system gradually tends to be stable; a larger mesh damping ratio can make the gear system maintain a stable cyclic motion state, reduce the vibration during gearing and prolong the service life of the gear system.

4 Conclusion

In this paper, based on the principle of thermal deformation, a nonlinear dynamics model of the gear system considering the temperature effect is established, and the bifurcation characteristics of the nonlinear system are analyzed by bifurcation diagram, maximum Lyapunov exponent diagram, time domain diagram, phase diagram, spectrum diagram and Poincare cross section diagram, and the following conclusions are obtained.

(1) The simulation reveals the effect law of temperature on the bifurcation characteristics of the system under different time-varying stiffness coefficients. For the dynamics model established in this paper, when the time-varying stiffness coefficient takes a small value ($s = 0.1$), the effect of temperature variation on the system motion is small, and the gear system keeps a stable single-fold cycle motion as the temperature increases. When the time-

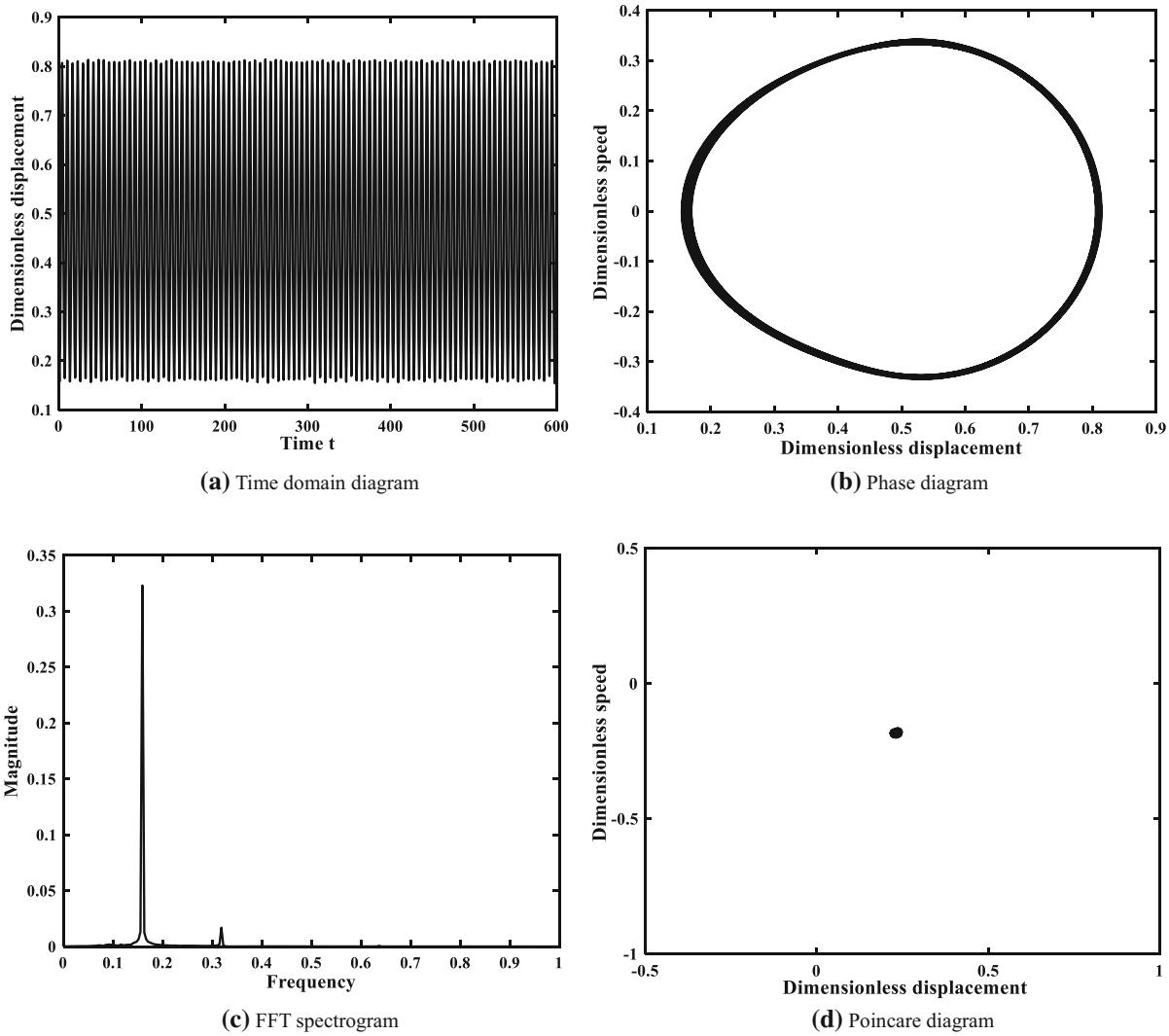

(a) Time domain diagram

(b) Phase diagram

(c) FFT spectrogram

(d) Poincare diagram

Fig. 20 Dynamic characteristics of the gear system with the mesh damping ratio $\xi = 0.18(\Delta T_1 = 50\ ^\circ C)$

varying stiffness factor is significant ($s = 0.6$), the effect of temperature variation on the system motion is more significant. The system undergoes a "two times—four times—two times " periodic motion change with the increase of temperature, and there is a bifurcation phenomenon.

(2) The effect of the time-varying stiffness coefficient on the bifurcation characteristics of the gear system at a fixed temperature rise ($\Delta T_1 = 50\ ^\circ C$) is analyzed. As the time-varying stiffness coefficient increases, the gear system moves from a single-cycle motion to a brief period three motion, which then changes to a period two motion. The system then undergoes a bifurcation into a period four motion, then enters a brief chaotic state, and following the system changes again into a period two motion. As the time-varying stiffness coefficient continues to increase, the gear system finally enters a chaotic state.

(3) The dynamical properties of the gear system are studied when the meshing damping ratio is used as a bifurcation parameter under the condition that the temperature variation is kept constant ($\Delta T_1 = 50\ ^\circ C$). The findings indicate that the kinematic state of the system gradually stabilizes with the increase of the meshing damping

ratio. A larger damping ratio can keep the system in a steady state of movement, reduce the vibration generated by the operation of the gear system, and extend its life of the gear system.

Funding This work was supported by the National Natural Science Foundation of China under Grant No.51765020 and the Natural Science Foundation of Jiangxi Province under Grant No. 20161BAB206153.

Declarations

Conflict of interest The authors report there are no competing interests to declare.

Data availability The data that support the findings of this study are available from the corresponding author, Jg W, upon reasonable request.

References

1. Wang, S.Y., Zhu, R.P.: Nonlinear torsional dynamics of star gearing transmission system of GTF gearbox. Shock. Vib. **2020**, 15 (2020). https://doi.org/10.1155/2020/6206418
2. Zhao, Y., Ahmat, M., Bari, K.: Nonlinear dynamics modeling and analysis of transmission error of wind turbine planetary gear system. Proc. Inst. Mech. Eng. Part K-J. Multi-Body Dyn. **228**(4), 438–448 (2014). https://doi.org/10.1177/1464419314536888
3. Hou, L., Cao, S.: Nonlinear dynamic analysis on planetary gears-rotor system in geared turbofan engines. Int. J. Bifurc. Chaos (2019). https://doi.org/10.1142/s0218127419500767
4. Jiang, Y., Zhu, H., Li, Z., Peng, Z.: The nonlinear dynamics response of cracked gear system in a coal cutter taking environmental multi-frequency excitation forces into consideration. Nonlinear Dyn. **84**(1), 203–222 (2016)
5. Chen, J., Li, W., Xin, G., Sheng, L., Jiang, S., Li, M.: Nonlinear dynamic characteristics analysis and chaos control of a gear transmission system in a shearer under temperature effects. Proc. Inst. Mech. Eng. Part C-J. Mech. Eng. Sci. **233**(16), 5691–5709 (2019). https://doi.org/10.1177/0954406219854112
6. Huang, K., Yi, Y., Xiong, Y.S., Cheng, Z.B., Chen, H.: Nonlinear dynamics analysis of high contact ratio gears system with multiple clearances. J. Braz. Soc. Mech. Sci. Eng. **42**(2), 16 (2020). https://doi.org/10.1007/s40430-020-2190-0
7. Ju, Z., Shuang, L., Xueyun, L.: Study on nonlinear dynamics of gearbox transmission system considering multiple influencing factors. Chinese J. Appl. Mech. **38**(02), 794–801 (2021)
8. Wang, J.Y., Wang, H.T., Wang, H., Guo, L.X.: Influence of the random system parameters on the nonlinear dynamic characteristics of gear transmission system. Int. J. Nonlinear Sci. Numer. Simul. **18**(7–8), 619–630 (2017). https://doi.org/10.1515/ijnsns-2016-0119
9. Geng, Z.B., Xiao, K., Li, J.Y., Wang, J.X.: Bifurcation and chaos of a spur gear transmission system with non-uniform wear. J. Vib. Acoustics-Trans. Asme **143**(3), 11 (2021). https://doi.org/10.1115/1.4048269
10. Liu, F.H., Jiang, H.J., Liu, S.N., Yu, X.H.: Dynamic behavior analysis of spur gears with constant and variable excitations considering sliding friction influence. J. Mech. Sci. Technol. **30**(12), 5363–5370 (2016). https://doi.org/10.1007/s12206-016-1103-8
11. Liu, H., Yan, P.F., Gao, P.: Effects of temperature on the time-varying mesh stiffness, vibration response, and support force of a multi-stage planetary gear. J. Vib. Acoustics-Trans. Asme **142**(5), 15 (2020). https://doi.org/10.1115/1.4047246
12. Wang, J., Yao, Z., Hassan, M. F., Zhao, Y.: Modeling and dynamics simulation of spur gear system incorporating the effect of lubrication condition and input shaft crack. Engineering Computations, ahead-of-print(ahead-of-print). (2021). https://doi.org/10.1108/EC-03-2021-0183
13. Wang, J.Y., Wang, H.T., Guo, L.X.: Analysis of stochastic nonlinear dynamics in the gear transmission system with backlash. Int. J. Nonlinear Sci. Numer. Simul. **16**(2), 111–121 (2015). https://doi.org/10.1515/ijnsns-2014-0089
14. Xiang, L., Deng, Z.Q., Hu, A.J.: Dynamical analysis of planetary gear transmission system under support stiffness effects. Int. J. Bifurc. Chaos **30**(6), 13 (2020). https://doi.org/10.1142/s0218127420500807
15. Xiang, L., Gao, N., Hu, A.J.: Dynamic analysis of a planetary gear system with multiple nonlinear parameters. J. Comput. Appl. Math. **327**, 325–340 (2018). https://doi.org/10.1016/j.cam.2017.06.021
16. Li, D., Shaw, S.W.: The effects of nonlinear damping on degenerate parametric amplification. Nonlinear Dyn. **102**(4), 2433–2452 (2020)
17. Neumeyer, S., Sorokin, V., van Gastel, M., Thomsen, J.J.: Frequency detuning effects for a parametric amplifier. J. Sound Vib. **445**, 77–87 (2019)
18. Neumeyer, S., Sorokin, V., Thomsen, J.J.: Effects of quadratic and cubic nonlinearities on a perfectly tuned parametric amplifier. J. Sound Vib. **386**, 327–335 (2017)
19. Zhu, Z.B., Cheng, L.C., Xu, R., Zhu, R.P.: Impacts of backlash on nonlinear dynamic characteristic of encased differential planetary gear train. Shock. Vib. **2019**, 15 (2019). https://doi.org/10.1155/2019/9347925
20. Pan, W., Li, X., Wang, L., Yang, Z.: Nonlinear response analysis of gear-shaft-bearing system considering tooth contact temperature and random excitations. Appl. Math. Model. **68**, 113–136 (2019). https://doi.org/10.1016/j.apm.2018.10.022
21. Pan, W., Ling, L., Qu, H., Wang, M.: Early wear fault dynamics analysis method of gear coupled rotor system based on dynamic fractal backlash. J. Comput. Nonlinear Dyn. (2021). https://doi.org/10.1115/1.4052650
22. Yang, Z., Bowen, C., Zhijie, X., Dalei, L.: Nonlinear dynamic analysis of a multi-degree-of-freedom gear system based on temperature effect. Modern Manuf. Eng. (05), 1–8 (2020)
23. Geng, Z.B., Xiao, K., Wang, J.X., Li, J.Y.: Investigation on nonlinear dynamic characteristics of a new rigid-flexible gear transmission with wear. J. Vib. Acoustics-Trans. Asme (2019). https://doi.org/10.1115/1.4043543

24. Wang, S., Zhu, R.: Modeling and theoretical investigation of nonlinear torsional characteristics for double-helical star gearing system in GTF gearbox. J. Vib. Eng. Technol. **10**(1), 193–209 (2022). https://doi.org/10.1007/s42417-021-00371-1
25. Li, S., Wu, Q.M., Zhang, Z.Q.: Bifurcation and chaos analysis of multistage planetary gear train. Nonlinear Dyn. **75**(1–2), 217–233 (2014). https://doi.org/10.1007/s11071-013-1060-z
26. Han, L., Guo, F.: Global sensitivity analysis of transmission accuracy for RV-type cycloid-pin drive. J. Mech. Sci. Technol. **30**(3), 1225–1231 (2016). https://doi.org/10.1007/s12206-016-0226-2
27. Li, Y.G., Chen, T.: Influence of the random system parameters on the nonlinear dynamic characteristics of gear transmission system. G., Wang, X. P. Non-linear dynamics of gear pair with dynamic backlash subjected to combined internal and external periodic excitations. J. Vib. Control, **22**(6), 1693–1703 (2016). https://doi.org/10.1177/1077546314544350
28. Xia, Y., Wan, Y., Liu, Z.Q.: Bifurcation and chaos analysis for a spur gear pair system with friction. J. Braz. Soc. Mech. Sci. Eng. **40**(11), 19 (2018). https://doi.org/10.1007/s40430-018-1443-7